JOC The Journal of Organic Chemistry

Article

pubs.acs.org/joc

DFT Study on the Mechanism and Stereoselectivity of NHC-Catalyzed Synthesis of Substituted Trifluoromethyl Dihydropyranones with Contiguous Stereocenters

Xiaoli Zhang, Mingsheng Tang, Yang Wang, Yingying Ran, Donghui Wei, Yanyan Zhu, and Wenjing Zhang*

The College of Chemistry and Molecular Engineering, Zhengzhou University, Zhengzhou, Henan Province 450001, P. R. China

Supporting Information

ABSTRACT: Recently, Smith and co-workers reported an interesting work that provides a facile approach to access substituted trifluoromethyl dihydropyranones with two contiguous stereocenters by utilizing the α,β-unsaturated trifluoromethyl ketones as a substrate for NHC-catalyzed [4 + 2] cycloadditions. The most significant point of this reaction lies in the capability of introducing substituents to the C(5) position of the dihydropyranones. In the present study, we performed detailed DFT investigations toward the catalytic mechanism of this reaction, and determined origins of the diastereo- and enatioselectivities through analyses on distortion energies of two key stationary species and on components of Gibbs free energy barriers of elementary steps in which the stereocenters are generated. The theoretically predicted configuration of the main product was well-consistent with the experimental results, and the excellent correlation between the relative free energy barriers ($\Delta\Delta G^0_{298}$) with the relative enthalpy barriers ($\Delta\Delta H^0_{298}$) indicates that the stereoselectivity should originate from differences of enthalpy barriers rather than distinctions of the entropy item ($-T\Delta S^0_{298}$) changes. The systematic study of the substituent effect affords conclusive evidence for the catalytic mechanism we proposed but failed to give any clue to how the various electronic properties of substituents act on the experimental yields.

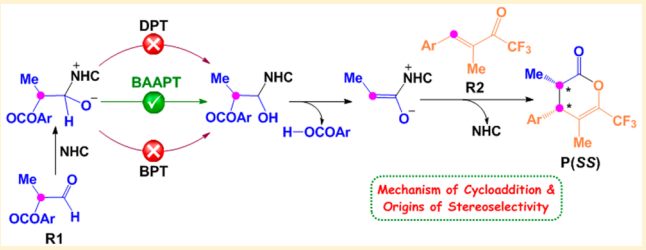

1. INTRODUCTION

The asymmetric synthesis of compounds containing contiguous stereocenters has attracted extensive attention of scientists working on catalytic and chemical research because these motifs are so prevalent in nature, and the synthesis of them is quite challenging.[1] Over the past few decades, numerous studies have demonstrated the excellent performances of *N*-heterocyclic carbenes (NHCs) acting as organocatalysts in asymmetric synthesis, such as the cross-benzoin,[2,3] Stetter,[4,5] annulation,[6] homoenolate,[7,8] and cycloaddition (in particular, including [2 + 2],[9−14] [2 + 2 + 2],[15] and [4 + 2][16−19]) reactions. The α-aroyloxyaldehydes in particular have been widely used to provide the acyl azolium under NHC catalysis, which allows the synthesis of both esters and amides in good yield, and the azolium enolate (derived from "Breslow-type" intermediate), which is able to undergo the formal [4 + 2] cycloadditions with *N*-aryl-*N*′-aroyldiazines or α,β-unsaturated β-trifluoroketones.[20−22]

Regarding NHC-catalyzed cycloadditions, which have been developed as one of the key approaches to access hetero or nonhetero cyclic asymmetric compounds, currently reported works cast most focus on utilizing β-substituted α,β-unsaturated ketones, ketimines, or aldimines as substrates of the specific NHC-catalyzed [4 + 2] cycloadditions. Several research groups chose to use α,β-substituted α,β-unsaturated ketones because the additional α-substituent could help to introduce substituents at the C(5) position of the dihydropyranone. The state-of-the-art works within this area were implemented by Kobayashi and Chi group (reactions (a) and (b) in Scheme 1),[23,24] but the substituents at the C(5) position of the dihydropyranone were limited to the activated bicarbonyl or aromatic ketone functionalities. Recently, α,β-unsaturated aldehydes were demonstrated to be able to react with imidazolidinone under catalysis of NHC to yield lactones (reaction (c) in Scheme 1),[25] and the azolium enolates accessed from ketenes have also been reported to be able to react with α-substituted enones (reaction (d) in Scheme 1).[18,26,27] The common limitation of these two azolium-enolate-type reactions lies in the fixed fused cycle substituents at the C(5) position of the pyranone systems. As seen from those perspectives, the work recently reported by Smith[28] indicates significant progress in asymmetric synthesis of dihydropyranones. They used α-aroyloxyaldehyde **1** and α,β-substituted α,β-unsaturated trifluoromethyl ketones **2** as substrates of the NHC-catalyzed cycloadditions to access substituted trifluoromethyl dihydropyranones (Scheme 2). The most interesting points of this reaction lie in the capability of introducing substituents,

Received: October 22, 2015
Published: December 30, 2015

DOI: 10.1021/acs.joc.5b02439
J. Org. Chem. 2016, 81, 868−877

Scheme 1. Previously Reported NHC-Catalyzed [4 + 2] Cycloadditions Utilizing Azoliumenolate Chemistry to Access Substituted Pyranones with Optical Activation

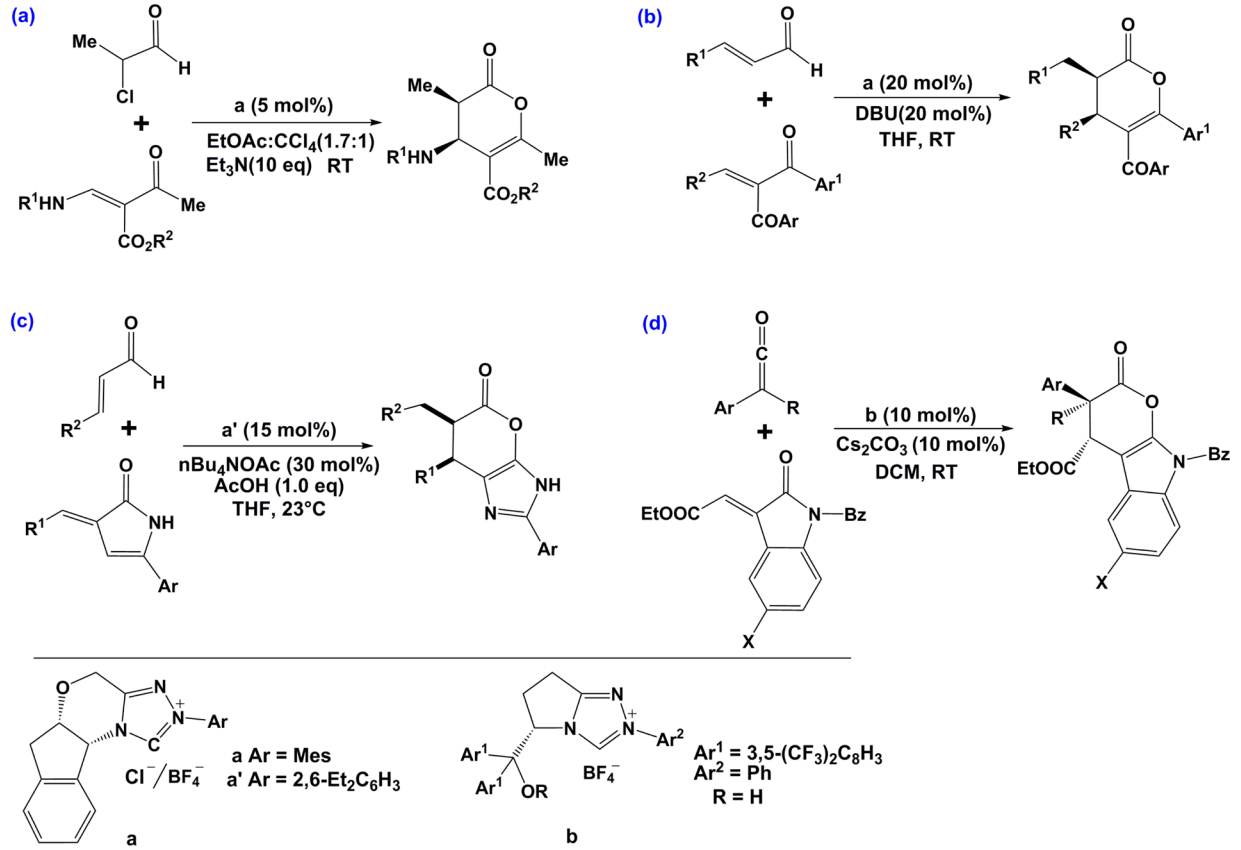

Scheme 2. NHC-Catalyzed [4 + 2] Cycloadditions Developed by Smith et al. to Access Substituted Trifluoromethyl Dihydropyranones

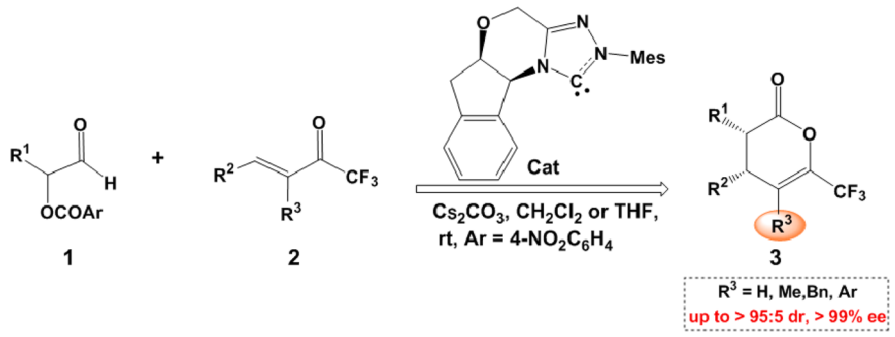

including methyl, benzyl, and aryl, to the C(5) position of the dihydropyranones, and the access of contiguous stereocenters with excellent diastereo- and enantioselectivity.

Inspired by theoretical studies presented by Bode and Kozlowski,[29] Smith and co-workers proposed a possible catalytic mechanism for the reaction displayed in Scheme 2. They proposed four general stages for the whole catalytic cycle (Scheme 3), in particular the nucleophilic attack of NHC catalyst to α-aroyloxyaldehyde **1**, followed by a proton transfer to generate "Breslow-type" intermediate **II**; the sequential elimination of a *p*-nitrobenzoate group and azolium enol proton with a step-by-step mechanism, resulting in formation of the azolium enol intermediate **III** and azolium enolate intermediate **IV**, respectively; the [4 + 2] cycloaddition according to a concerted, but highly asynchronous, hetero-Diels−Alder reaction process; and finally, the elimination of the free NHC catalyst to release the final product and complete the catalytic cycle.

The systematic theoretical study toward the NHC-catalyzed reaction of α,β-unsaturated aldehydes reported by Bode and Kozlowski[29] was indeed inspirational considering the systematic nature of the work and the novel interesting conclusions they achieved: (i) the [4 + 2] cycloaddition occurs through a concerted, but highly asynchronous, hetero-Diels−Alder reaction rather than the stepwise Michael- or Classen-type pathways; (ii) two crucial interactions, in particular the oxyanion-steering mechanism and the CH-π interaction, were identified to enable the high stereoselectivity. The problem is that all those conclusions were stated to be obtained on the basis of computational results at the IEFPCM-HF/6-31G(d)//

DOI: 10.1021/acs.joc.5b02439
J. Org. Chem. 2016, 81, 868−877

Scheme 3. Proposed Catalytic Cycle of the NHC-Catalyzed [4 + 2] Cycloaddition by Smith et al.

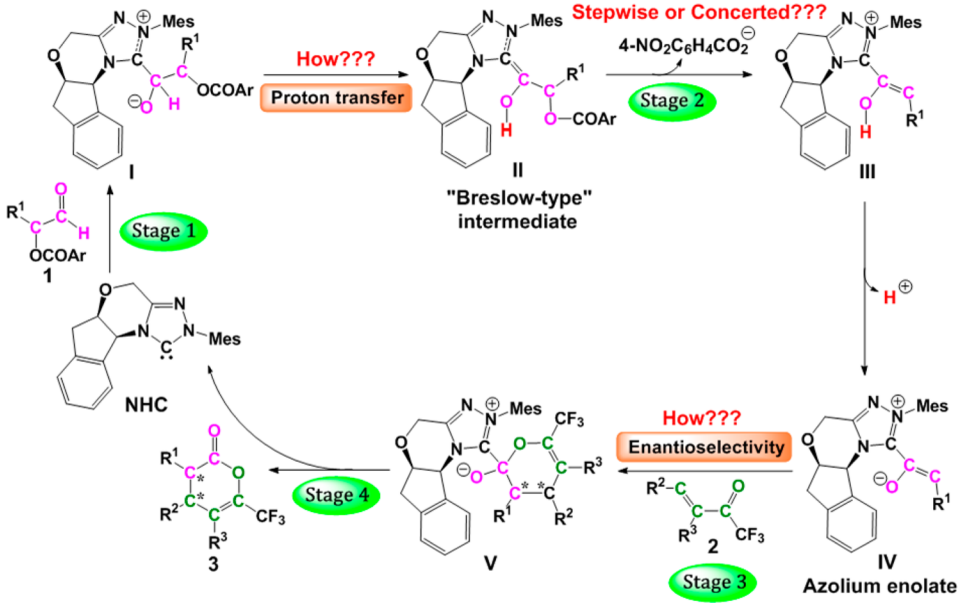

HF/6-31G(d) level of theory.[30−32] As we all know, the Hartree−Fock method can be viewed as a special density functional that includes 100% Hartree−Fock exchange functional and no correlation, and neglecting electron correlation can lead to serious deviations from experimental results,[33,34] and this is why so many post-Hartree−Fock methods (CC,[35,36] MP_n,[37] CI,[38] QCI,[39] CASSCF,[40−42] etc.) have been proposed to improve the computational results.

A most successful alternative to the Hartree−Fock method is density functional theory (DFT),[43] which includes both exchange and correlation energies. Over the past few decades, the DFT method has been widely used in mechanism and stereoselectivity studies toward organic and catalytic reactions,[16,44,45] and a number of DFT approximations have been demonstrated to be able to give rational explanations for experimental phenomena and accurate predictions on the optical properties of the final products. In particular, one of the global hybrid meta-GGA (meta-generalized gradient approximation) functional, namely M06-2X,[33,46,47] which was developed by the Truhlar group, has been widely demonstrated to perform very well on both energy and geometry predictions toward systems consisting of main group elements only. Therefore, in the present study, we will pursue a detailed DFT investigation on the mechanism and stereoselectivity of the title catalytic reaction by utilizing the M06-2X functional.

Furthermore, Bode and Kozlowski[29] did not provide the complete energy profile for the reactions they studied. They optimized several key transition states for the Diels−Alder reaction mechanism at the HF/6-31G(d) level, calculated the relative free energies of those transition states, and then identified the most favorable configuration of the final product, which was consistent with the experimental result. However, except for the diastereo- and enantioselectivity, there are still several key issues of the Diels−Alder reaction mechanism that are ambiguous before we make the whole energy profile very clear, as shown in Scheme 3, for example: (i) the direct 1,2-H shift and the 1,3-H shift processes have been definitely verified to be very difficult. Then in Stage 1, how should the proton be transferred from the aldehyde carbon atom to the aldehyde oxygen atom to yield the famous "Breslow-type" intermediate **II**? (ii) In Stage 2, will the carboxylate ion $4\text{-}NO_2C_6H_4CO_2^-$ and the proton H^+ be removed through a stepwise or concerted mechanism? (iii) In Stage 3, the stage to generate the two contiguous stereocenters, although Bode and Kozlowski have identified the oxyanion steering and CH-π interactions as two key factors for the enantio- and diastereoselectivity, we need further confirmation with a much more reliable computational method, such as the M06-2X functional of the DFT method, and a much more intensive study to explore if there are more fundamental reasons for generation of the optical activity centers. (iv) Will substituents with different electron properties (electron-donating or -withdrawing) influence yields of the reaction? With all these questions as motivation, the present work will pursue a detailed DFT investigation of the title reaction to not only access a complete free energy potential profile for the NHC-catalyzed [4 + 2] cycloaddition reaction of α-aroyloxyaldehydes with a more reliable computational method but also explore the mechanism of the "Breslow-type" intermediate formation and the factors that likely control the stereochemistry of the title reaction. We believe that the mechanistic information provided in this study should be important for offering guidance to better understand the NHC-catalyzed [4 + 2] cycloaddition reaction with α-aroyloxyaldehydes as substrates at the molecular level and provide some novel insights into origins of the generation of stereoselectivity.

2. COMPUTATIONAL DETAILS

2.1. Model Selection. We chose the theoretical investigation models after very careful and comprehensive evaluations toward the experimental results, including the time the reaction takes, and the yields and stereoselectivities obtained by utilizing corresponding reactants. As a result, 2-*p*-nitrobenzoyloxy-2-methyl-acetaldehyde (R^1 = Me, Scheme 2) and 1-trifluoromethyl-2-methyl-3-(*p*-nitrophenyl)-prop-2-en-1-one (R^2 = *p*-nitrophenyl, R^3 = Me, Scheme 2) were selected as the objects of our investigation. For the sake of convenience, we will denote the NHC catalyst used in experiments as **Cat**, and compounds 2-*p*-nitrobenzoyloxy-2-methyl-acetaldehyde and 1-trifluoromethyl-2-methyl-3-(*p*-nitrophenyl)-prop-2-en-1-one as **R1** and **R2**, respectively, in the rest of this paper.

2.2. Computational Details. All density functional theory (DFT) calculations were performed using the Gaussian 09 suite of

DOI: 10.1021/acs.joc.5b02439
J. Org. Chem. 2016, 81, 868−877

Scheme 4. Possible Reaction Mechanism for the Title Catalytic Cycloaddition

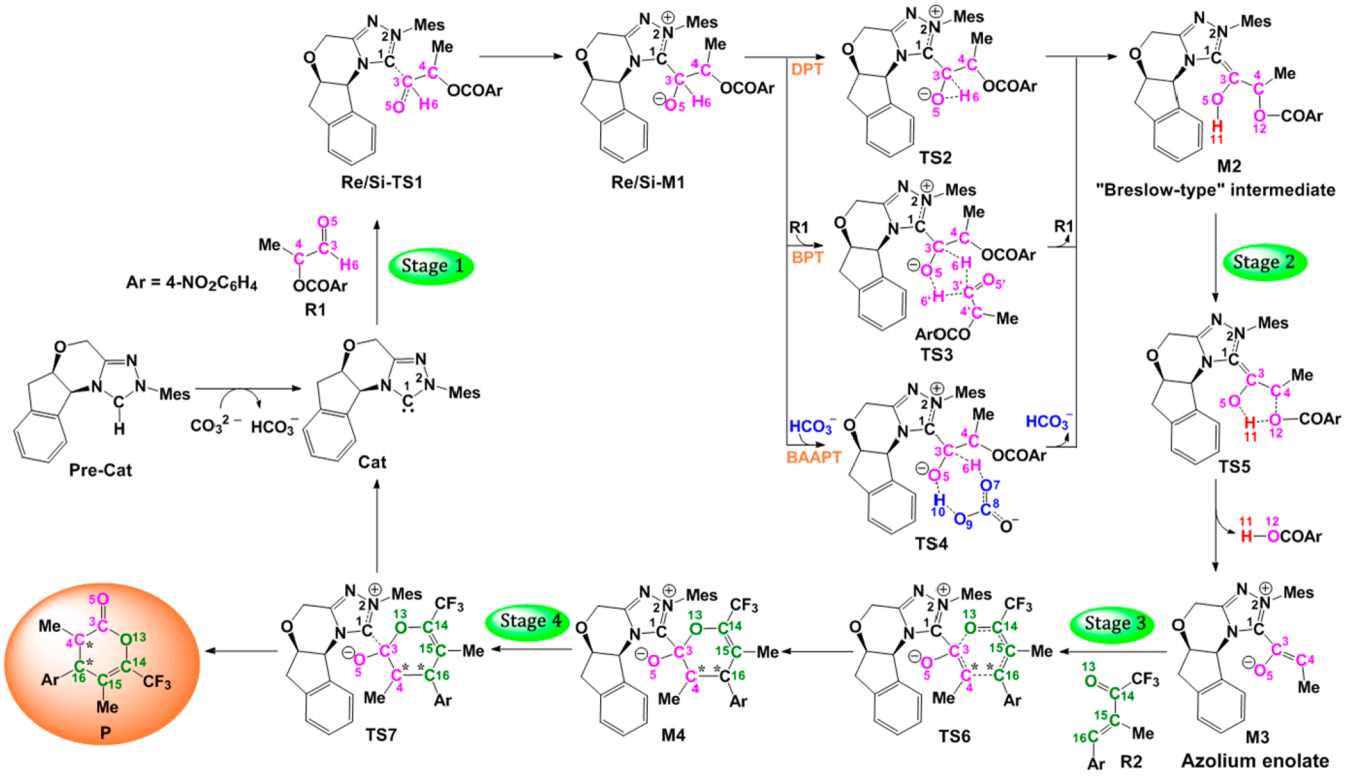

programs.[48] The geometries of all the reactants, transition states, intermediates, and products were fully optimized in gas phase by using the M06-2X density functional with the 6-31G(d, p) basis set. The vibrational frequencies, which were used to help ensure each transition state has one and only one imaginary frequency while all of the reactants, intermediates, and products have no imaginary frequency, were calculated at the same level with the temperature set as 298.15 K and the pressure as 1 atm. The same level of intrinsic reaction coordinate (IRC)[49,50] calculations were performed to confirm each transition state leads to the expected reactants and products.

On the basis of the optimized structures obtained in gas phase, the single-point energies were further refined at the M06-2X/6-31++G(d, p) level of theory with the solvent effects of THF simulated by the polarizable continuum model using the integral equation formalism variant (IEFPCM). All discussions in the present paper were based on the calculated Gibbs free energies, which were the electronic (including nuclear-repulsion) energies calculated at the IEFPCM-M06-2X/6-31++G(d, p)//M06-2X/6-31G(d, p) level of theory plus the thermal corrections to Gibbs free energies calculated in gas phase with M06-2X functional and the 6-31G(d, p) basis set.

To test the suitability of the M06-2X/6-31G(d, p)//6-31++G(d, p)//IEFPCM$_{THF}$ method, we have performed full optimizations for some selected stationary points by using the M06-2X/6-31++G(d, p)//IEFPCM$_{THF}$ method, and the results are summarized in Part 3 of the Supporting Information, where we can observe that the optimized geometries in gas phase and in implicit solvent have small differences, and the relative energy from these optimization calculations is in good agreement with the refined value with a deviation of 0.5 kcal/mol. Thus, we believe the selected computational method in the present work should be suitable and reliable for investigations of the studied reaction system.[51]

3. RESULTS AND DISCUSSION

3.1. Catalytic Mechanism. On the basis of the mechanism suggested by Smith,[28] the theoretical investigations reported by Bode and Kozlowski,[29] and the previous DFT studies on the NHC-catalyzed cycloadditions performed by our own group,[16,44,45] we proposed a possible reaction mechanism for the title catalytic [4 + 2] cycloaddition and illustrated it in Scheme 4. As can be seen, the whole catalytic cycle that occurs after the formation of the real catalyst **Cat** in situ from the triazole compound **Pre-Cat** with the assistance of CO_3^{2-} (derivative from the base of Cs_2CO_3) was proposed to go through four stages, i.e., the formation of the "Breslow-type" intermediate **M2** through two elementary steps, in particular the combination of NHC catalyst **Cat** with the *α*-aroyloxyaldehyde **R1**, and sequentially the 1,2-H transfer from the C3 to O5 atom; elimination of the *p*-nitrobenzoic acid by a concerted elementary step to give the azolium enolate intermediate **M3**; [4 + 2] cycloaddition via the Diels−Alder reaction mechanism, i.e., the concerted cycloaddition mechanism, to give intermediate **M4**; and finally, the elimination of product **P** along with regeneration of the NHC catalyst. In the following parts of this section, we will present detailed discussions for each stage.

3.1.1. Stage 1: Formation of the "Breslow-type" Intermediate. Before we begin to discuss the mechanism in further detail, we have to emphasize that it is indeed important and also challenging to make clear which reactant the catalyst would initially interact with when one tries to investigate the mechanism of a catalytic cycloaddition process.[16,44,45] However, in this work, we did not study the mechanism in which the catalytic cycle is initiated by nucleophilic attack of the NHC catalyst to the diene (*α,β*-unsaturated trifluoromethylketone **R2**) because the "Breslow-type" intermediate that is formed by reaction of NHC with aldehyde has been definitively verified by Breslow and others.[24,29,52,53]

As shown in Scheme 4, with assistance from CO_3^{2-} (derivative from the base of Cs_2CO_3), deprotonation of the triazole compound **Pre-Cat** occurs to yield the active catalyst **Cat** accompanied by the generation of a molecule of HCO_3^-,

DOI: 10.1021/acs.joc.5b02439
J. Org. Chem. 2016, 81, 868−877

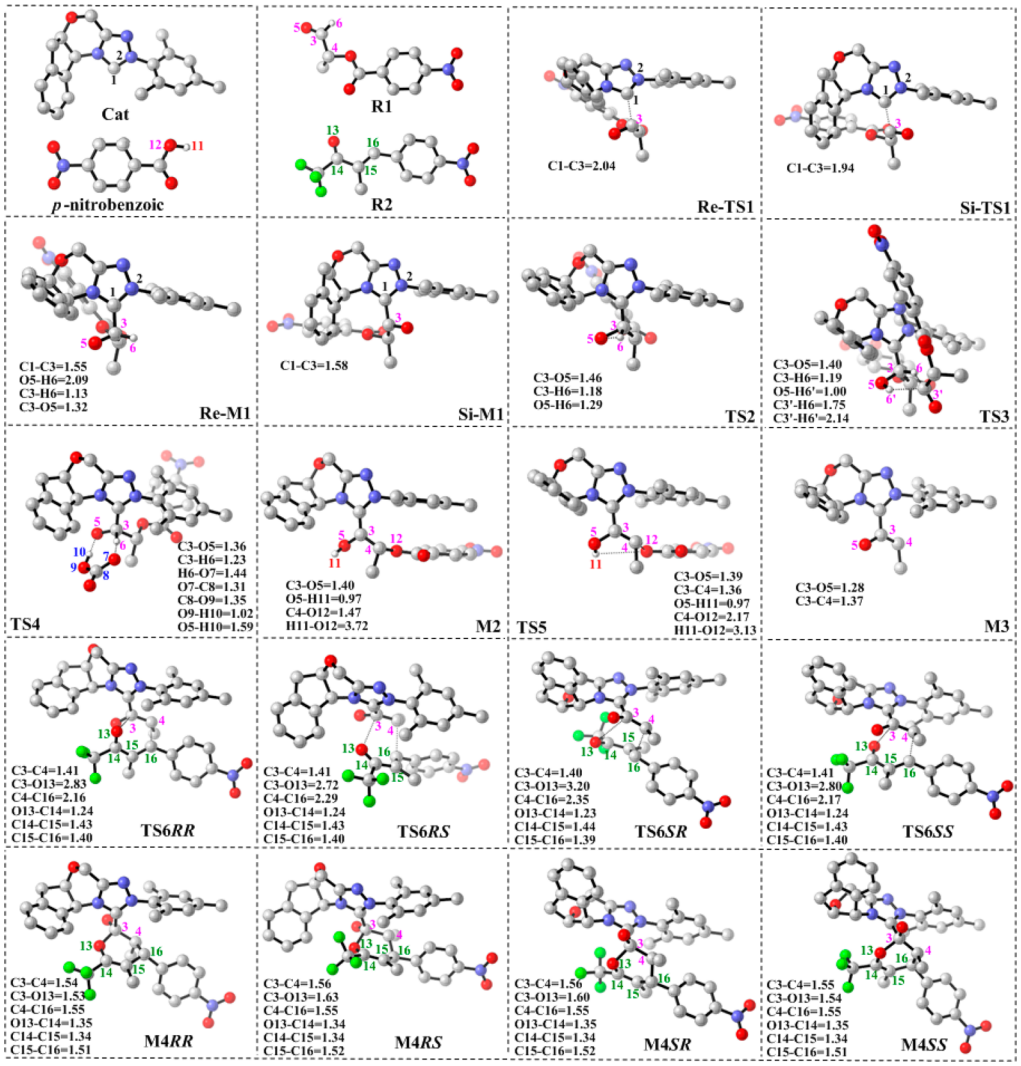

Figure 1. Optimized geometries of all stationary points involved in the title NHC-catalyzed [4 + 2] cycloaddition. All bond lengths are given in Å, and all three-dimensional structures are represented using CYLView.[56]

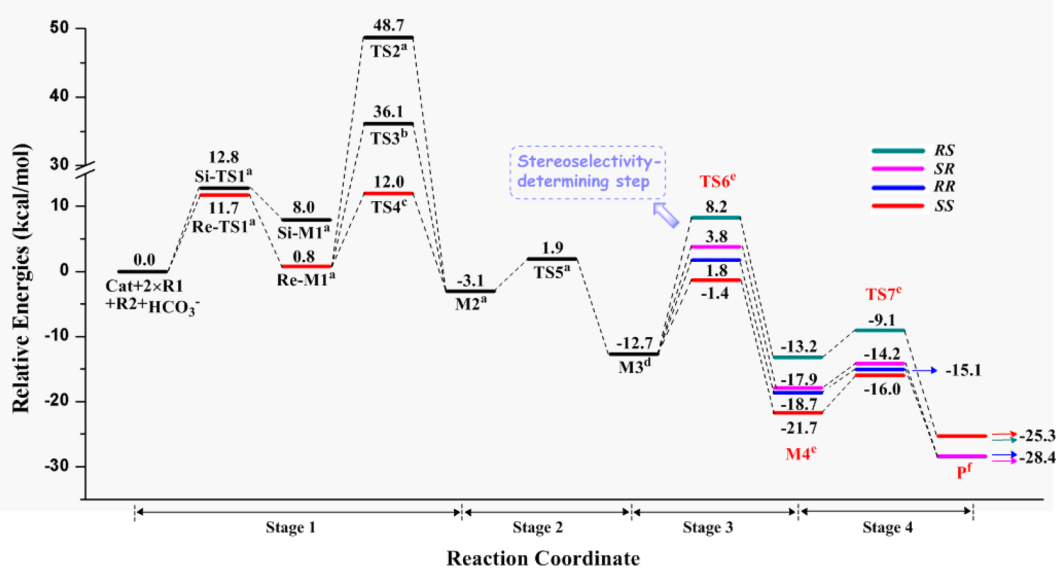

Figure 2. Gibbs free energy profiles of the title NHC-catalyzed [4 + 2] cycloaddition adding the energies of (a) **R2**+**R1**+HCO_3^-, (b) **R2**+HCO_3^-, (c) **R2**+**R1**, (d) **R2**+**R1**+HOCOAr+HCO_3^-, (e) **R1**+HOCOAr+HCO_3^-, and (f) **R1**+**Cat**+HOCOAr+HCO_3^-.

DOI: 10.1021/acs.joc.5b02439
J. Org. Chem. 2016, 81, 868−877

the conjugate acid of CO_3^{2-}.[54,55] Then, the coordinated zwitterionic intermediate **Re-M1** or **Si-M1** (denoted as **Re/Si-M1**) is formed through the nucleophilic attack of the C1 atom in **Cat** to the C3 atom in reactant **R1** from its *Re* or *Si* face via transition states **Re/Si-TS1**, respectively. The optimized geometries presented in Figure 1 show that the distance between C1 and C3 atoms reduces from 2.04/1.94 Å in **Re/Si-TS1** to 1.55/1.58 Å in **Re/Si-M1**, respectively, which implies the complete combination of **Cat** with **R1**. Figure 2 displays the Gibbs free energy profile for the whole reaction, and the energies of **Cat**+2 × **R1**+**R2**+HCO_3^- were set as the reference of 0.0 kcal/mol. From Figure 2, we can easily determine that the barrier via **Re-TS1** is 1.1 kcal/mol lower than that via **Si-TS1**, and more importantly, the adduct intermediate **Re-M1** locates 7.2 kcal/mol lower than **Si-M1**, indicating that the nucleophilic attack of **Cat** to the *Re* face of **R1** is both thermodynamically and kinetically favorable to that to the *Si* face. Therefore, for the rest of the calculations, we will drop all reactions associated with **Si-M1**.

The second step of Stage 1 is to transfer proton H6 from the C3 to O5 atom to yield the "Breslow-type" intermediate **M2** (Scheme 4). Following a typical 1,2-H shift process, a highly strained three-membered ring structure would present in the transition state of this direct proton transfer (DPT) pathway, which will probably induce a highly unreasonable reaction energy barrier. Then, inspired by previous investigations conducted by our own and other's groups,[57−60] we proposed another two possible pathways: the bimolecular proton transfer (BPT) pathway with assistance of another molecule of *α*-aroyloxyaldehyde **R1** and the bicarbonate anion-assisted proton transfer (BAAPT) pathway with HCO_3^-, which is the byproduct of the reaction of **Pre-Cat** with the base Cs_2CO_3 (Scheme 4) acting as the medium. The transition states for the DPT, BPT, and BAAPT pathways are denoted as **TS2**, **TS3**, and **TS4**, respectively.

(i) DPT pathway: The optimized geometry of **TS2** shows consistent structure with what we mentioned above, i.e., a three-membered ring (C3-O5-H6) structure appears. The distance between O5 and H6 atoms is shortened from 2.09 Å in **Re-M1** to 1.29 Å in **TS2**, whereas the bond lengths of C3−H6 and C3−O5 are elongated from 1.13 and 1.32 Å in **Re-M1** to 1.18 and 1.46 Å in **TS2**, respectively. These changes definitely indicate the formation of the three-membered ring structure in **TS2**. Please note that we gave the hydrogen atom bonded to O5 atom a completely new number (i.e., H11) in **M2** and all structures after because this atom comes from different molecules via different pathways. The free energy barrier of this direct proton transfer pathway was calculated to be as high as 47.9 kcal/mol, which is apparently difficult to overcome at room temperature.

(ii) BPT pathway: Inspired by the recent DFT study[58] carried out by our own group toward the NHC-catalyzed dimerization of methyl methacrylate, we proposed a bimolecular proton transfer mechanism that is assisted by another molecule of **R1**. In particular, upon another **R1** approaching intermediate **Re-M1**, the H6′ atom is shifted from the C3′ atom to the O5 atom, and the H6 atom is transferred from the C3 atom to the C3′ atom. All of these reactive centers built a five-membered ring in transition state **TS3** via which the Gibbs free energy barrier is significantly lowered (35.3 kcal/mol) compared with that through the DPT pathway, but it is still too high to be overcome under the experimental conditions. The optimized geometry of **TS3** clearly shows that these two proton transfers are highly asynchronous, and the shift of H6′ atom happens earlier than that of the H6 atom.

(iii) BAAPT pathway: The BAAPT pathway is actually also a bimolecular proton transfer pathway, but it uses the bicarbonate anion as the proton transfer medium. The proposal of this pathway was also inspired by one of our recent studies[16] in which we demonstrated that the bicarbonate anion-assisted proton transfer is much more energetically favorable than that of the direct proton transfer mechanism or the water-assisted transfer mechanism. As shown in Scheme 4, in the BAAPT pathway, the H6 atom is transferred from the C3 atom to the carbonyl oxygen atom O7, and the hydrogen atom H10 of the monoacid is shifted from the O9 atom to the O5 atom. The transition state of this process is denoted as **TS4**, which includes a seven-membered ring structure (C3-H6-O7-C8-O9-H10-O5). The free energy barrier of the BAAPT pathway is only 11.2 kcal/mol, which is much lower than that of the BPT pathway and quite easy to be overcome under the experimental conditions. The main reason for the much lower energy barrier through the BAAPT pathway than that of the BPT pathway could be attributed to the smaller stretching force derived from the seven-membered ring of transition state **TS4** than that derived from the five-membered ring of transition state **TS3**.

Taking all three possible proton transfer pathways into consideration, the most energetically favorable pathway is found to be the one assisted by bicarbonate anion, and the Gibbs free energy barrier is located to be only 11.2 kcal/mol, which is very easily overcome under the experimental conditions. The much lower barrier of the BAAPT pathway should be partly attributed to expansion of the ring that consists of corresponding reactive centers from the three-membered in **TS2** or five-membered in **TS3** to seven-membered in **TS4**, which significantly reduces the stretching forces that derived from the ring structures contained in the transition states.

3.1.2. Stage 2: Formation of the Azolium Enolate. Stage 2 is to remove a molecule of *p*-nitrobenzoic acid from the "Breslow-type" intermediate **M2** and then access azolium enolate intermediate **M3**. Smith and co-workers proposed a stepwise mechanism for this process, meaning that the intermediate **M2** would first eliminate the *p*-nitrobenzoate anion to leave an azolium enol and then dismiss the hydrogen cation to access azolium enolate **M3**. However, our theoretical computational results indicate a concerted mechanism via transition state **TS5** (Scheme 4), and the IRC calculations absolutely demonstrate that **TS5** could lead to the earlier intermediate **M2** and the later intermediate **M3** plus *p*-nitrobenzoic acid.

The geometrical parameters depicted in Figure 1 show that the cleavage of the C4−O12 bond is more advanced than the formation of the H11−O12 bond, revealing a concerted but highly asynchronous manner. The length of the C4−O12 bond is elongated from 1.47 Å in **M2** to 2.17 Å in **TS5**, whereas the distance between the H11 and O12 atoms is shortened from 3.72 Å in **M2** to 3.13 Å in **TS5** and finally 0.97 Å in *p*-nitrobenzoic acid, which definitely indicates the full formation of the H11−O12 bond. The energy barrier of this elementary step is 5.0 kcal/mol, which is quite easy to overcome at room temperature.

3.1.3. Stage 3: [4 + 2] Cycloaddition. In Stage 3, the hetero-Diels−Alder [4 + 2] cycloaddition occurs between the azolium enolate **M3** and the trifluoromethyl-substituted *α*,*β*-unsaturated ketone **R2**. As shown in Scheme 4, the C4 atom in **M3** attacks the C16 atom in diene **R2**, and the O13 atom in **R2** attacks the

DOI: 10.1021/acs.joc.5b02439
J. Org. Chem. 2016, 81, 868−877

C3 atom in **M3**, resulting in the formation of two chemical bonds C4−C16 and C3−O13 in intermediate **M4** via the transition state **TS6**. In particular, the bonding of the C4 and C16 atoms would result in formation of two contiguous chiral carbon centers, i.e., the C4 and C16 atoms, and four configurations would possibly present in corresponding products through the four additional patterns that are illustrated in Scheme 5. As shown, the azolium enolate intermediate **M3** can possibly attack either the *Re* or *Si* face of diene **R2** with its own *Re* or *Si* face.

Scheme 5. Illustration of the Cycloaddition Patterns of M3 with R2

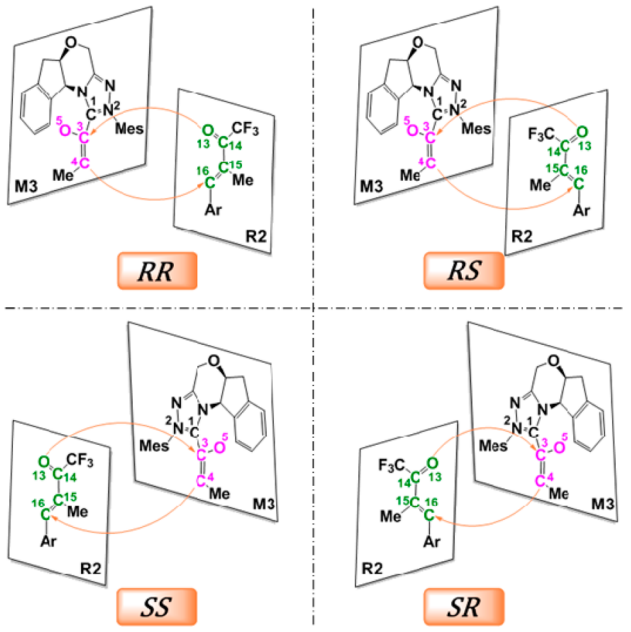

We denote the four transition states that appear in this [4 + 2] cycloaddition step correspondingly as **TS6*RR***, **TS6*SS***, **TS6*SR***, and **TS6*RS***; the first "***R***" or "***S***" represents the chirality of the C4 atom, and the latter "***R***" or "***S***" represents the chirality of the C16 atom. As we can observe from the optimized geometries of the four transition states given in Figure 1, the C4−C16 and C3−O13 bonds are formed asynchronously, and formation of the C4−C16 bond happens earlier than that of the C3−O13 bond. However, the IRC calculations for those transition states definitely demonstrate a concerted mechanism. In other words, our theoretical calculations stand on the point that the [4 + 2] cycloaddition occurs in a concerted but asynchronous manner, which is consistent with what was concluded by Bode and Kozlowski.[29] The barrier via **TS6*SS*** is only 11.3 kcal/mol (Figure 2), which is obviously lower than barriers via any of the other transition states. This result indicates good agreement with the experimental results that the most favorable product is in *SS* configuration. Moreover, the energy barriers via **TS6*RR*** and **TS6*SS*** are both lower than those via **TS6*SR*** and **TS6*RS***, which is perfectly consistent with the experimental diastereomeric ratio (>95:5).

3.1.4. Stage 4: Regeneration of the Catalyst. In the last stage, the product is released with the cleavage of the C1−C3 bond accompanied by regeneration of the NHC catalyst. The four transition states (**TS7*RR***, **TS7*SS***, **TS7*SR***, and **TS7*RS***) via which the dissociations occur were all located, and their geometries are given in Figure 1. The elongation of the C1−C3 bond length from **M7**s to **TS7**s definitely indicates this dissociation process, and the gradual shortening of the C3−O5 bond length from **M7**s to **TS7**s, and finally the product **P**s, indicates the full formation of the C3═O5 double bond.

The free energy barriers via **TS7*SS***, **TS7*RR***, **TS7*SR***, and **TS7*RS*** are 5.7, 3.6, 3.7, and 4.1 kcal/mol, respectively, where we can see that the dissociation reaction via **TS7*SS*** is not most energetically favorable, but the energy barrier of 5.7 kcal/mol is quite easy to overcome to form the corresponding product **P*SS***. More importantly, the stereoselectivities have been determined in the [4 + 2] cycloaddition process such that a little bit higher barrier in this step would not have any effect on the favorable configuration of the final product.

3.2. Origin of Stereoselectivity. To make clear the origin of the generation of stereoselectivity from a theoretical perspective is of great value for experimental scientists to pertinently synthesize asymmetric compounds with desired optical activation. With respect to the specific reaction we are studying in the current work, the contiguous stereocenters (C4 and C16 atoms) are formed within the hetero-Diels−Alder [4 + 2] cycloaddition process; thus, this elementary step should be the key step to determine the stereoselectivities of the reaction. Therefore, we first performed analysis on the distortion energies (E_{dist})[61] of **M3** and **R2**, which refer to the energy changes from their stable geometries to the geometries as they are in transition states **TS6*SS***, **TS6*RR***, **TS6*SR***, and **TS6*RS***, respectively. We also performed analysis on components of Gibbs free energy barriers via **TS6**s. Analyses conducted with these two methodologies are effective approaches to access deep understanding of the molecule interactions from an indirect perspective, clearly determine the main components that contribute to barriers via each transition state, and determine the main reasons that different barriers result from different transition states, especially for those transition states with similar structures (e.g., diastereo- and enantioisomers). The computational results are shown in Tables 1 and 2.

Table 1. Contributions of Distortion Energies (E_{dist}) of M3 and R2 to Energy Barriers via TS6s[a]

	E_{dist} (**M3**)	E_{dist} (**R2**)	E_{dist} (sum)
TS6*SS*	10.7	11.6	22.3
TS6*RR*	12.8	11.6	24.4
TS6*SR*	6.1	8.7	14.8
TS6*RS*	13.7	10.1	23.8

[a]The last column lists the sum of the two distortion energies. All energies were calculated at the M06-2X/6-31G(d,p) level of theory in gas phase (kcal/mol).

Table 2. Free Energy Barriers via TS6s and their Corresponding Components[a]

	ΔG^0_{298}	ΔH^0_{298}	$-T\Delta S^0_{298}$	$\Delta\Delta G^0_{298}$	$\Delta\Delta H^0_{298}$
TS6*SS*	11.3	−6.2	17.5	0.0	0.0
TS6*RR*	14.5	−4.2	18.7	3.2	1.9
TS6*SR*	16.5	−1.4	17.9	5.2	4.8
TS6*RS*	20.9	+3.5	17.4	9.6	9.7

[a]The last two columns give the relative free energy barriers and the relative enthalpy changes (kcal/mol).

DOI: 10.1021/acs.joc.5b02439
J. Org. Chem. 2016, 81, 868−877

From the calculated distortion energies shown in Table 1, we can see that, for each of the four transition states, the contributions derived from geometry distortions of **M3** are in similar magnitude with that from **R2**. Specifically, E_{dist}(**R2**) is a little bit larger than E_{dist}(**M3**) via transition states **TS6*SS*** and **TS6*SR***, whereas it is a little bit smaller than E_{dist}(**M3**) via transition states **TS6*RR*** and **TS6*RS***. The total distortion energies (E_{dist}(sum)) via **TS6*SS*** have similar magnitudes with, but smaller than, those via **TS6*RR*** and **TS6*RS***, which is in line with the sense of stereoselectivity reported in experiments.[28] Considering the lowest barrier via **TS6*SS*** discussed above, we can reasonably speculate that the interaction energies between the **R2** and **M3** moieties in **TS6*SS*** should be larger than those in **TS6*RR*** and **TS6*RS***. The only special case is **TS6*SR*** because the E_{dist}(sum) via it is obviously smaller than those of the other three, which we consider should be attributed to the larger distance between the **R2** and **M3** moieties, because with similar energy barriers, the larger the distance between the moieties, the weaker the interactions probably are. From the optimized geometries shown in Figure 1, we can see that the distances between the C3 and O13 atoms and C4 and C16 atoms in **TS6*SS***, **TS6*RR***, and **TS6*RS*** are 2.72−2.83 Å and 2.16−2.29 Å, respectively, which are significantly shorter than 3.20 and 2.35 Å, respectively, in **TS6*SR***; thus, relatively weaker interactions between **M3** and **R2** moieties in **TS6*SR*** could be reasonably expected.

In other words, according to analysis of the distortion energies of **M3** and **R2** from their stable geometries to those in transition states **TS6**s, we can reasonably speculate that the smaller distortion energies should contribute to the lower energy barrier via **TS6*SS***, and the larger distance between **M3** and **R2** moieties in **TS6*SR*** leads to weaker distortion effects, which raise the molecule energy, but simultaneously, the larger distance also leads to obviously weaker interactions, which are propitious to reduce molecular energy. The final result of these two contradictory effects is to lead to higher energy barrier via **TS6*SR*** than that via **TS6*SS***.

From the calculated Gibbs free energy barriers and their components for the [4 + 2] cycloaddition process that are presented in Table 2, we conclude that, for each transition state, contributions to free energy barriers from the change of entropy item ($-T\Delta S^0_{298}$) are considerably larger than enthalpy (ΔH^0_{298}), but the entropy changes from reactants of this step (i.e., **M3** and **R2**) to the four transition states are quite similar. Therefore, the differences of free energy barriers via the four transition states originate mainly from differences of the enthalpy barriers rather than those of entropy. In other words, the origin of stereoselectivities of the title reaction should be identified to the different enthalpy changes when the reaction goes through different transition states.

To make clearer illustrations of the crucial effects of the close relationship between ΔH^0_{298} and ΔG^0_{298} toward the stereoselectivities of the reaction, we calculated the relative free energy barriers ($\Delta\Delta G^0_{298}$) and relative enthalpy barriers ($\Delta\Delta H^0_{298}$) as compared to their corresponding values via **TS6*SS***. The results are listed in the last two columns of Table 2, from which we can easily find that, for each transition state, the value of $\Delta\Delta G^0_{298}$ is roughly identical with that of $\Delta\Delta H^0_{298}$. We also tried to represent them with a correlation linear, which is displayed in Figure 3. The calculated slope and the Pearson correlation coefficient for this line equal 1.027 and 0.982, respectively, which remarkably confirm the same variety trend of $\Delta\Delta G^0_{298}$ with that of $\Delta\Delta H^0_{298}$ and furthermore demonstrates

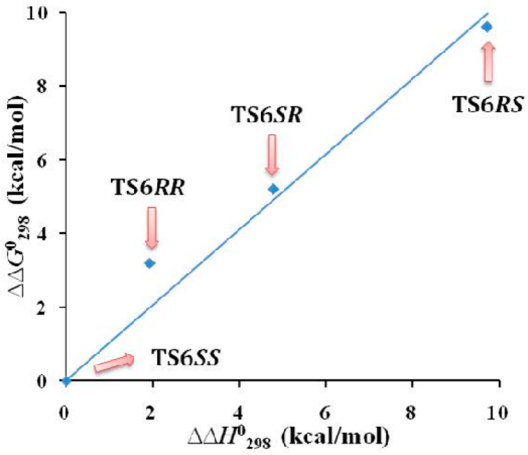

Figure 3. Correlation of the relative free energy barriers ($\Delta\Delta G^0_{298}$) with the relative enthalpy barriers ($\Delta\Delta H^0_{298}$) for the [4 + 2] cycloaddition step. Please note that the free energy barrier and enthalpy barrier of transition state **TS6*SS*** were set as 0.0 kcal/mol.

the significant contributions of differences of enthalpy barriers to stereoselectivities of the cycloaddition reaction. More interestingly, the **TS6*RR*** was found to obviously deviate from the line, which we believe should be attributed to the relatively larger entropy change (18.7 kcal/mol, Table 2) via **TS6*RR*** compared to those via the other three transition states, and this could be further attributed to its relative larger distortion energy shown in Table 1 (24.4 kcal/mol).

3.3. Substituent Effects. Reactions of *α*-aroyloxyaldehyde with various *α*,*β*-unsaturated trifluoromethyl ketones (with the *α*-substituent being 4-BrC_6H_4, 4-$NO_2C_6H_4$, 4-FC_6H_4, or 4-$MeOC_6H_4$) were systematically studied to explore the substituent effects. We calculated the Gibbs free energy barriers ΔG^0_{298} of the concerted [4 + 2] cycloaddition process when using different *α*-substituted ketones because all reactions before this elementary step are the same (Scheme 4).

Table 3 lists the computational results of ΔG^0_{298} and the experimental yields. From these results we can observe that,

Table 3. Calculated Gibbs Free Energy Barriers of the [4 + 2] Cycloaddition Step and the Experimental Yields with Different *α*-Substituents in Ketone Ordered by Magnitude of ΔG^0_{298}

entry	*α*-substituents	ΔG^0_{298}(kcal/mol)	yield (%)
1	4-BrC_6H_4	10.2	97
2	4-$NO_2C_6H_4$	11.3	84
3	4-FC_6H_4	19.1	66
4	4-$MeOC_6H_4$	23.2	65

with different *α*-substituted ketones as the reactants, the yield would decrease with increasing free energy barriers. To illustrate this tendency in a more intuitional way, we plotted a scattergram of the reaction yield versus the calculated ΔG^0_{298}, and displayed it in Figure 4. Clearly, the free energy barrier is in inverse correlation with the experimental yield. This is a reasonable correlation, and simultaneously, this correlation provides conclusive evidence for the mechanism we proposed. Nevertheless, this systematic study failed to afford any clue to the regular effects of properties of substituents (electron-withdrawing or -donating) toward the experimental yield because the yield or energy barrier does not vary regularly

DOI: 10.1021/acs.joc.5b02439
J. Org. Chem. 2016, 81, 868−877

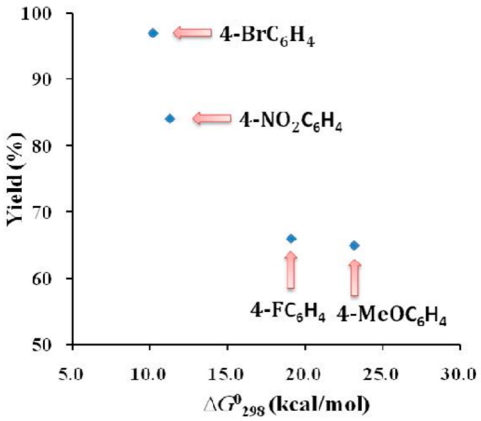

Figure 4. Scattergram of the experimental yields versus the calculated ΔG^0_{298}.

with the increase (or decrease) of the electron-withdrawing (or -donating) ability of the corresponding substituent.

4. CONCLUSIONS

The DFT study using the M06-2X functional has been carried out to investigate the detailed mechanism and stereoselectivity of the NHC-catalyzed [4 + 2] cycloadditions to synthesize highly functionalized dihydropyranones utilizing *α,β*-substituted *α,β*-unsaturated trifluoromethyl ketones as substrate. Our theoretical calculations demonstrate four stages that are necessary for the whole catalytic cycle, in particular, formation of the "Breslow-type" intermediate (Stage 1), formation of the azolium enolate (Stage 2), [4 + 2] cycloaddition (Stage 3), and finally regeneration of the catalyst (Stage 4). Among these four stages, Stage 1 includes two elementary steps, i.e., the nucleophilic attack of NHC catalyst to the reactant *α*-aroyloxyaldehyde **R1** and the 1,2-H transfer. The calculated results show that the bicarbonate anion-assisted proton transfer (BAAPT) pathway with HCO_3^- as the proton medium is significantly energetically favorable relative to the direct proton transfer (DPT) pathway or the bimolecular proton transfer (BPT) pathway. Stage 3 is verified to be the stereoselectivity-determining step, and the adduct product with *SS* configuration is most favorable for the yield, which is well-consistent with the experimental results. Finally, the analysis on the distortion energies of **M3** and **R2** indicates that the relatively smaller distortion energies of those two species along with the relatively larger interactions between the **M3** and **R2** moieties in **TS6***SS* finally lead to the main product in *SS* configuration. The analysis on Gibbs free energy barriers and their components of the [4 + 2] cycloaddition process shows that the different free energy barriers ($\Delta\Delta G^0_{298}$) via the four **TS6**s originate from the different enthalpy barriers ($\Delta\Delta H^0_{298}$), and the changes of the entropy items ($-T\Delta S^0_{298}$) via all **TS6**s are almost equal.

On the basis of all discussions stated above, we demonstrate that the trace amount of bicarbonate anions are important because they perform very well as a novel proton medium, and conclude that it is the difference of enthalpy barriers via transition states with different configurations that contribute to the different free energy barriers and furthermore contribute to stereoselectivity of the reaction. The systematic study of reactions using various *α*-substituted ketones as the reactant demonstrated the inverse correlation between the experimental yield and the free energy barrier, and this reasonable correlation afforded further verification of the catalytic mechanism we proposed, but we failed to find any clue as to the regular effect of the electronic nature on the reactivity. This work provides valuable guidance for future theoretical and experimental investigations toward NHC-catalyzed asymmetric cycloadditions.

■ ASSOCIATED CONTENT

Supporting Information

The Supporting Information is available free of charge on the ACS Publications website at DOI: 10.1021/acs.joc.5b02439.

List of absolute Born−Oppenheimer energies (*E*), Gibbs free energies (*G*) and enthalpies (*H*) (in hartree, Part 1), optimized geometries of stationary points involved in the substituent effects (Part 2), comparisons of relative energies calculated by full optimization in implicit solvent with those by single-point refinement (Part 3), test of B3LYP functional (Part 4), and Cartesian coordinates of all stationary points involved in this study (Part 5) (PDF)

■ AUTHOR INFORMATION

Corresponding Author

*E-mail: zhangwj@zzu.edu.cn.

Notes

The authors declare no competing financial interest.

■ ACKNOWLEDGMENTS

The work described in this study was supported by the National Natural Science Foundation of China (Nos. 21503191 and 21303167), China Postdoctoral Science Foundation (No. 2015M572115), and University Key Research Program of Henan Province (Nos. 14A150033 and 15A150082).

■ REFERENCES

(1) Nicolaou, K. C.; Edmonds, D. J.; Bulger, P. G. *Angew. Chem., Int. Ed.* **2006**, *45*, 7134−7186.
(2) Enders, D.; Grossmann, A.; Fronert, J.; Raabe, G. *Chem. Commun.* **2010**, *46*, 6282−6284.
(3) Ema, T.; Oue, Y.; Akihara, K.; Miyazaki, Y.; Sakai, T. *Org. Lett.* **2009**, *11*, 4866−4869.
(4) DiRocco, D. A.; Rovis, T. *J. Am. Chem. Soc.* **2011**, *133*, 10402−10405.
(5) Jousseaume, T.; Wurz, N. E.; Glorius, F. *Angew. Chem., Int. Ed.* **2011**, *50*, 1410−1414.
(6) Lee, A.; Scheidt, K. A. *Chem. Commun.* **2015**, *51*, 3407−3410.
(7) Lu, H.; Liu, J. Y.; Li, C. G.; Lin, J. B.; Liang, Y. M.; Xu, P. F. *Chem. Commun.* **2015**, *51*, 4473−4476.
(8) Chen, X. K.; Fang, X. Q.; Chi, Y. R. *Chem. Sci.* **2013**, *4*, 2613−2618.
(9) Wang, X. N.; Shao, P. L.; Lv, H.; Ye, S. *Org. Lett.* **2009**, *11*, 4029−4031.
(10) Huang, X. L.; Chen, X. Y.; Ye, S. *J. Org. Chem.* **2009**, *74*, 7585−7587.
(11) Douglas, J.; Taylor, J. E.; Churchill, G.; Slawin, A. M. Z.; Smith, A. D. *J. Org. Chem.* **2013**, *78*, 3925−3938.
(12) Wang, X. N.; Shen, L. T.; Ye, S. *Org. Lett.* **2011**, *13*, 6382−6385.
(13) Wang, T.; Huang, X. L.; Ye, S. *Org. Biomol. Chem.* **2010**, *8*, 5007−5011.
(14) Zhang, H. M.; Gao, Z. H.; Ye, S. *Org. Lett.* **2014**, *16*, 3079−3081.
(15) Wang, X. N.; Shen, L. T.; Ye, S. *Chem. Commun.* **2011**, *47*, 8388−8390.
(16) Wang, Y.; Zheng, L.; Wei, D.; Tang, M. *Org. Chem. Front.* **2015**, *2*, 874−884.

DOI: 10.1021/acs.joc.5b02439
J. Org. Chem. 2016, 81, 868−877

(17) Leckie, S. M.; Brown, T. B.; Pryde, D.; Lebl, T.; Slawin, A. M. Z.; Smith, A. D. *Org. Biomol. Chem.* **2013**, *11*, 3230−3246.
(18) Jian, T. Y.; Chen, X. Y.; Sun, L. H.; Ye, S. *Org. Biomol. Chem.* **2013**, *11*, 158−163.
(19) Jian, T. Y.; Shao, P. L.; Ye, S. *Chem. Commun.* **2011**, *47*, 2381−2383.
(20) Ling, K. B.; Smith, A. D. *Chem. Commun.* **2011**, *47*, 373−375.
(21) Davies, A. T.; Taylor, J. E.; Douglas, J.; Collett, C. J.; Morrill, L. C.; Fallan, C.; Slawin, A. M. Z.; Churchill, G.; Smith, A. D. *J. Org. Chem.* **2013**, *78*, 9243−9257.
(22) Taylor, J. E.; Daniels, D. S. B.; Smith, A. D. *Org. Lett.* **2013**, *15*, 6058−6061.
(23) Kobayashi, S.; Kinoshita, T.; Uehara, H.; Sudo, T.; Ryu, I. *Org. Lett.* **2009**, *11*, 3934−3937.
(24) Fang, X.; Chen, X.; Chi, Y. R. *Org. Lett.* **2011**, *13*, 4708−4711.
(25) McCusker, E. O.; Scheidt, K. A. *Angew. Chem., Int. Ed.* **2013**, *52*, 13616−13620.
(26) Lv, H.; You, L.; Ye, S. *Adv. Synth. Catal.* **2009**, *351*, 2822−2826.
(27) Lv, H.; Chen, X. Y.; Sun, L. H.; Ye, S. *J. Org. Chem.* **2010**, *75*, 6973−6976.
(28) Davies, A. T.; Pickett, P. M.; Slawin, A. M. Z.; Smith, A. D. *ACS Catal.* **2014**, *4*, 2696−2700.
(29) Allen, S. E.; Mahatthananchai, J.; Bode, J. W.; Kozlowski, M. C. *J. Am. Chem. Soc.* **2012**, *134*, 12098−12103.
(30) Sang-Aroon, W.; Ruangpornvisuti, V. *Int. J. Quantum Chem.* **2008**, *108*, 1181−1188.
(31) Tomasi, J. M.; Cancés, B. *J. Mol. Struct.: THEOCHEM* **1999**, *464*, 211−226.
(32) Hehre, W. J. D.; Pople, J. A. *J. Chem. Phys.* **1972**, *56*, 2257−2261.
(33) Zhang, W.; Truhlar, D. G.; Tang, M. *J. Chem. Theory Comput.* **2013**, *9*, 3965−3977.
(34) Zhang, W.; Truhlar, D. G.; Tang, M. *J. Chem. Theory Comput.* **2014**, *10*, 2399−2409.
(35) Pople, J. A.; Krishnan, R.; Schlegel, H. B.; Binkley, J. S. *Int. J. Quantum Chem.* **1978**, *14*, 545−560.
(36) Bartlett, R. J.; Purvis, G. D. *Int. J. Quantum Chem.* **1978**, *14*, 561−581.
(37) Møller, C.; Plesset, M. S. *Phys. Rev.* **1934**, *46*, 618−622.
(38) Foresman, J. B.; Head-Gordon, M.; Pople, J. A.; Frisch, M. J. *J. Phys. Chem.* **1992**, *96*, 135−149.
(39) Pople, J. A.; Head-Gordon, M.; Raghavachari, K. *J. Chem. Phys.* **1987**, *87*, 5968.
(40) Hegarty, D.; Robb, M. A. *Mol. Phys.* **1979**, *38*, 1795−1812.
(41) Eade, R. H. A.; Robb, M. A. *Chem. Phys. Lett.* **1981**, *83*, 362−368.
(42) Schlegel, H. B.; Robb, M. A. *Chem. Phys. Lett.* **1982**, *93*, 43−46.
(43) Domingo, L. R.; Perez-Ruiz, R.; Arguello, J. E.; Miranda, M. A. *J. Phys. Chem. A* **2009**, *113*, 5718−5722.
(44) Zhang, W.; Zhu, Y.; Wei, D.; Li, Y.; Tang, M. *J. Org. Chem.* **2012**, *77*, 10729−10737.
(45) Wang, Y.; Wang, Y.; Zhang, W.; Zhu, Y.; Wei, D.; Tang, M. *Org. Biomol. Chem.* **2015**, *13*, 6587−6597.
(46) Zhao, Y.; Truhlar, D. G. *Theor. Chem. Acc.* **2008**, *120*, 215−241.
(47) Zhao, Y.; Truhlar, D. G. *Acc. Chem. Res.* **2008**, *41*, 157.
(48) Frisch, M. J.; Trucks, G. W.; Schlegel, H. B.; Scuseria, G. E.; Robb, M. A.; Cheeseman, J. R.; Scalmani, G.; Barone, V.; Mennucci, B.; Petersson, G. A.; Nakatsuji, H.; Caricato, M.; Li, X.; Hratchian, H. P.; Izmaylov, A. F.; Bloino, J.; Zheng, G.; Sonnenberg, J. L.; Hada, M.; Ehara, M.; Toyota, K.; Fukuda, R.; Hasegawa, J.; Ishida, M.; Nakajima, T.; Honda, Y.; Kitao, O.; Nakai, H.; Vreven, T.; Montgomery, J. A., Jr.; Peralta, J. E.; Ogliaro, F.; Bearpark, M.; Heyd, J. J.; Brothers, E.; Kudin, K. N.; Staroverov, V. N.; Keith, T.; Kobayashi, R.; Normand, J.; Raghavachari, K.; Rendell, A.; Burant, J. C.; Iyengar, S. S.; Tomasi, J.; Cossi, M.; Rega, N.; Millam, J. M.; Klene, M.; Knox, J. E.; Cross, J. B.; Bakken, V.; Adamo, C.; Jaramillo, J.; Gomperts, R.; Stratmann, R. E.; Yazyev, O.; Austin, A. J.; Cammi, R.; Pomelli, C.; Ochterski, J. W.; Martin, R. L.; Morokuma, K.; Zakrzewski, V. G.; Voth, G. A.; Salvador, P.; Dannenberg, J. J.; Dapprich, S.; Daniels, A. D.; Farkas, O.; Foresman, J. B.; Ortiz, J. V.; Cioslowski, J.; Fox, D. J. *Gaussian 09*, revision C. 01; Gaussian, Inc.: Wallingford, CT, 2010.
(49) Gonzalez, C.; Schlegel, H. B. *J. Chem. Phys.* **1989**, *90*, 2154.
(50) Gonzalez, C.; Schlegel, H. B. *J. Phys. Chem.* **1990**, *94*, 5523−5527.
(51) Huang, F.; Zhang, C.; Jiang, J.; Wang, Z. X.; Guan, H. *Inorg. Chem.* **2011**, *50*, 3816−3825.
(52) Breslow, R. *J. Am. Chem. Soc.* **1958**, *80*, 3719−3726.
(53) Glorius, F.; Hirano, K. *Organocatalysis* **2008**, *2*, 159−181.
(54) Mahatthananchai, J.; Bode, J. W. *Acc. Chem. Res.* **2014**, *47*, 696−707.
(55) Zhang, Q.; Yu, H.-Z.; Fu, Y. *Org. Chem. Front.* **2014**, *1*, 614−624.
(56) Legault, C. Y. *CYLview*, 1.0b, Université de Sherbrooke, 2009; http://www.cylview.org.
(57) Wang, Y.; Wei, D.; Zhang, W.; Wang, Y.; Zhu, Y.; Jia, Y.; Tang, M. *Org. Biomol. Chem.* **2014**, *12*, 7503−7514.
(58) Li, Y.; Zhu, Y.; Zhang, W.; Wei, D.; Ran, Y.; Zhao, Q.; Tang, M. *Phys. Chem. Chem. Phys.* **2014**, *16*, 20001−20008.
(59) Guo, X.; Zhang, L.-B.; Wei, D.; Niu, J.-L. *Chem. Sci.* **2015**, *6*, 7059−7071.
(60) Wang, Y.; Guo, X.; Tang, M.; Wei, D. *J. Phys. Chem. A* **2015**, *119*, 8422−8431.
(61) Legault, C. Y.; Garcia, Y.; Merlic, C. A.; Houk, K. N. *J. Am. Chem. Soc.* **2007**, *129*, 12664−12665.

DOI: 10.1021/acs.joc.5b02439
J. Org. Chem. 2016, 81, 868−877